

Samarium hexaboride: A trivial surface conductor

P. Hlawenka,¹ K. Siemensmeyer,¹ E. Weschke,¹ A. Varykhalov,¹ J. Sánchez-Barriga,¹ N. Y. Shitsevalova,²
A. V. Dukhnenko,² V. B. Filipov,² S. Gabáni,³ K. Flachbart,³ O. Rader,¹ and E. D. L. Rienks¹

¹*Helmholtz-Zentrum Berlin für Materialien und Energie,
Elektronenspeicherring BESSY II, Albert-Einstein-Straße 15, 12489 Berlin, Germany*

²*Institute for Problems of Materials Science, National Academy of
Sciences of Ukraine, Krzhynzhansky str. 3, 03142 Kiev, Ukraine*

³*Institute of Experimental Physics, Slovak Academy of Sciences, Watsonova 47, 04001 Košice, Slovakia*
(Dated: July 26, 2021)

Recent theoretical and experimental studies suggest that SmB₆ is the first topological Kondo insulator: A material in which the interaction between localized and itinerant electrons renders the bulk insulating at low temperature, while topological surface states leave the surface metallic. While this would elegantly explain the material's puzzling conductivity, we find the experimentally observed candidates for both predicted topological surface states to be of trivial character instead: The surface state at $\bar{\Gamma}$ is very heavy and shallow with a mere ~ 2 meV binding energy. It exhibits large Rashba splitting which excludes a topological nature. We further demonstrate that the other metallic surface state, located at \bar{X} , is not an independent in-gap state as supposed previously, but part of a massive band with much higher binding energy (1.7 eV). We show that it remains metallic down to 1 K due to reduced hybridization with the energy-shifted surface $4f$ level.

INTRODUCTION

Over the past decade, topological insulators have been established as a new state of matter [1]. Rather subtle symmetry attributes of the bulk band structure of these materials dictate the electronic structure at their surface: Gapless states with a particular spin polarization will inevitably exist at the confines of insulators that can be classified as topologically non-trivial.

The about 30 materials that have thus far been positively identified as members of this category [2] are well captured by a single electron description. In recent years, the focus has shifted towards the question whether the concept of topological insulators can be generalized to materials in which electron correlation plays a more prominent role. Two families of materials with increased correlation strength have been brought forward as promising candidates: Ir-based materials [3] and the Kondo insulators [4]. In the latter group, hybridization between a narrow f -level and the much wider conduction band leads to a small indirect band gap at low temperature. At appropriate band filling, the chemical potential falls within this gap, rendering the material an insulator. In the case of SmB_6 , the suggestion that it could be a topological insulator [4–15] has deservedly attracted a lot of attention, since it would also provide an elegant solution to the long-standing controversy about its unexpected residual conductivity at low temperature [16–20]. Could SmB_6 , after being identified as the first mixed valence system in the 1960s [21] and the first Kondo insulator shortly after [22–24], now become the exemplification of yet another phenomenon in solid state research?

Band structure calculations, treating correlation in various ways, do point in this direction [5–8]. A d - f band inversion at X is predicted to give rise to two distinct topological surface states: One at \bar{X} , appearing twice in the surface Brillouin zone, and the second at $\bar{\Gamma}$. Three Dirac cones are thus predicted, which would make SmB_6 a strong topological insulator. The cubic symmetry is further found to exclude it from having a phase with an even number of Dirac cones, i.e., from being a weak topological insulator [7].

The first strides on the experimental front were also seemingly successful towards establishing SmB_6 as the first topological Kondo insulator: It is indeed found that it behaves like a bulk insulator with a conductive surface at low temperature [25–27]. In addition, evidence of metallic surface states at the predicted sites, $\bar{\Gamma}$ and \bar{X} , has been found using angle-resolved photoemission spectroscopy (ARPES) [9–14, 28] and de Haas-van Alphen experiments [15].

Even though several aspects leave ample room for doubts, most notably the fact that no Dirac cones have been found and the much lower than expected effective mass [7], two reports have appeared that provide seemingly strong support in favor of the topological thesis: It is found that the introduction of magnetic impurities suppresses the residual low-temperature conductance [27]. Moreover, spin-polarized ARPES measurements appear to confirm the helical spin texture [12].

In spite of these results, we provide strong evidence that the surface states at the (100) surface of SmB_6 are topologically trivial: We first demonstrate that the —until now elusive— state at $\bar{\Gamma}$ is massive and exhibits Rashba splitting, excluding a topological nature. This result already leads to insurmountable disagreement with the theoretical predictions, since a topological surface state at $\bar{\Gamma}$ is required to arrive at an odd number of Dirac cones. In a second step we show that the well-characterized \bar{X} state is not an independent in-gap state as supposed previously. Instead, we show that it is part of a massive surface state with a binding energy (E_B) of 1.7 eV that derives from the bulk d -band at X . We demonstrate how this state hybridizes with the surface $4f$ level to yield a gap that is both smaller and shifted to higher binding energy with respect to its bulk counterpart.

While our findings thus provide an explanation for the long-standing puzzle of samarium hexaboride’s low temperature conductivity, they conflict very clearly with the idea that it would be the first realization of a strongly correlated topological insulator.

THE $\bar{\Gamma}$ STATE

In agreement with earlier ARPES studies [9–14, 28], we observe a state that forms an elliptical Fermi surface contour around the \bar{X} point. In addition, we can clearly resolve a shallow feature at the center of the surface Brillouin zone which has previously been considered a candidate for the Dirac cone at $\bar{\Gamma}$ [9–13, 28]. In Fig. 1 we show data for B and Sm terminated surfaces [29]. On the B terminated surface, this state has a handlebar moustache-like dispersion, reminiscent of a shallow, Rashba-split pair, see Figs. 1(a–c). The Rashba splitting is a spin-orbit effect [31] which lifts the spin degeneracy of two-dimensional states leading to an in-plane spin texture as indicated in Fig. 1. Alternatively, we point out that the observed dispersion also bears a resemblance with the topological surface state of Bi_2Te_3 . In that system the dispersion becomes non-linear immediately below the Dirac point and passes through two turning points before it meets with the valence band [32]. One could thus argue that what we observe is part of the dispersion of a topological surface state. We discard this possibility for two reasons. Firstly, we do not observe any evidence for

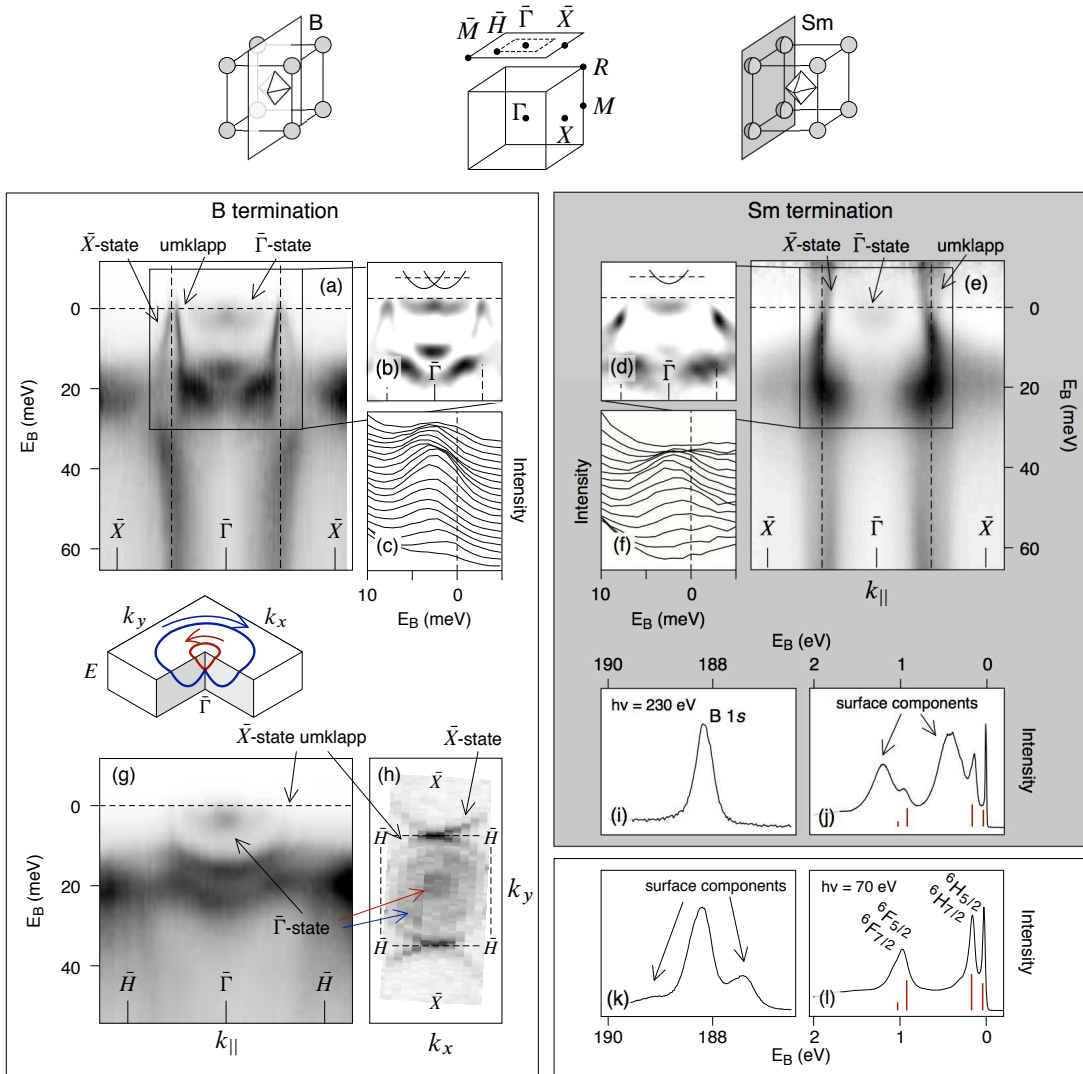


Figure 1. Massive nature and Rashba splitting of the $\bar{\Gamma}$ state. Photoemission intensity (I) along the $\bar{\Gamma}$ - \bar{X} direction for (a) B and (e) Sm terminated surfaces together with (b,d) second derivative (d^2I/dE^2). Solid lines in (b) (Rashba split) and (d) (not split) are parabolic dispersions derived from a fit of the photoemission intensity with a two-dimensional model of the spectral function (vertically offset). (c,f) $\bar{\Gamma}$ state represented as spectra. The data on the Sm terminated sample (d-f) were measured at 40 K to thermally populate a larger fraction of the shallow $\bar{\Gamma}$ state. The results have been divided by a Fermi-Dirac distribution. (g) Photoemission intensity along the $\bar{\Gamma}$ - \bar{H} - \bar{M} direction (to avoid contributions from the \bar{X} state) on the B terminated surface. (h) Fermi surface of a B terminated sample. (i,k) B 1s core level and (j,l) angle integrated valence band spectra for B and Sm terminated samples. Bars in (j,l) indicate calculated intensity for the $f^6 \rightarrow f^5$ (Sm^{2+}) photoemission transition [30]. $h\nu = 31$ eV and s-polarization, unless stated otherwise.

the dispersion bending down to connect to the valence band. This also holds when the state is traced along the $\bar{\Gamma}$ - \bar{M} direction where a downturn in the dispersion would not be obscured by the intensity of the \bar{X} state, Fig. 1(g). The second, more powerful argument is the termination dependence we observe. The $\bar{\Gamma}$ state appears as a single parabola on the Sm terminated surface, as shown in Fig. 1(d-f). This result strongly hints at Rashba splitting, because this effect relies on the gradient of the crystal potential perpendicular to the surface. Given the polar nature that bulk truncated surfaces with pure B or Sm termination would have, a difference in surface potential is very conceivable for the different terminations.

Interpreting the $\bar{\Gamma}$ state as a free electron-like state, we obtain a binding energy of 2.3 ± 0.6 meV and a very large effective mass of $\sim 35 m_e$. The Rashba parameter (α_R) amounts to $(1.9 \pm 0.2) \times 10^{-12}$ eV m on the B terminated surface. This very modest Rashba parameter further cements the idea that the splitting is controlled by a difference in surface potential between terminations: In systems where α_R is an order of magnitude larger, such as the L -gap

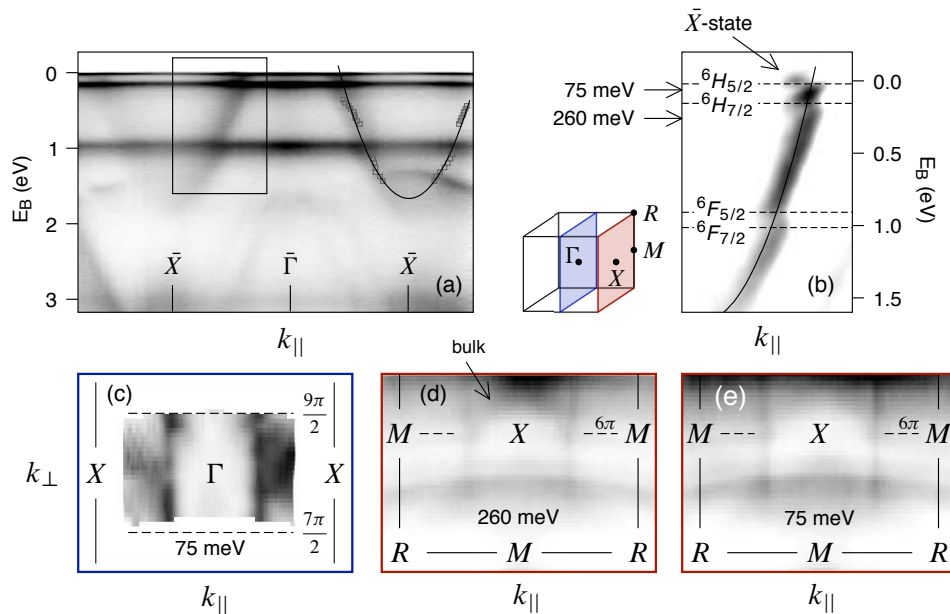


Figure 2. Massive, two-dimensional nature of the \bar{X} state. (a) Photoemission intensity along $\bar{X}-\bar{\Gamma}-\bar{X}$ obtained with $h\nu = 70$ eV. Markers indicate position of maxima in fits of momentum distribution curves, solid line is a parabolic fit to these points (markers and solid line horizontally offset by 2π). (b) Second derivative (d^2I/dk^2) of the area marked in (a). Energies of the f -orbital multiplets are indicated by dashed lines, arrows indicate the binding energies of $(k_{\parallel}, k_{\perp})$ maps shown in (c-e). Photoemission intensity on the $\Gamma-X-M$ (blue in the Brillouin zone sketch) and $X-M-R$ (red) planes at the indicated binding energies. The vertical features in (c-e) indicate two-dimensional character. All results obtained with p -polarization.

surface state on Au(111) with $\alpha_R = 3 \times 10^{-11}$ eV m, the observed splitting can still be influenced by changes in the surface potential [33]. In so-called giant Rashba systems where the Rashba parameter is an order of magnitude higher still ($\alpha_R \sim 10^{-10}$ eV m), the splitting is found unaffected even by large work function changes because it is more difficult to change the wavefunction asymmetry [34, 35]. It is thus conceivable that a relatively small change in the surface potential between terminations suffices to determine whether the $\bar{\Gamma}$ state exhibits Rashba splitting or not. Note that the splitting is only observable here by virtue of the very large effective mass, since $\Delta k_{\parallel} = m^* \alpha_R / \hbar^2$.

The large effective mass directly suggests that the $\bar{\Gamma}$ state stems from a bulk $4f$ state. Moreover, the intensity of the $\bar{\Gamma}$ state displays discrete maxima in the vicinity of the photon energies with which a Γ point can be reached and is next to invisible at all other photon energies. This further indicates that it is split off a bulk Γ state.

In summary, we find evidence for a massive surface state at the surface Brillouin zone center which can exhibit Rashba splitting. As we mentioned above, the absence of a topological surface state at $\bar{\Gamma}$ precludes SmB₆ from classification as a strong topological insulator, regardless of the nature of the other surface state at \bar{X} . In the following, however, we will also present a trivial explanation for this widely observed feature.

THE \bar{X} STATE

In agreement with published results [9–14, 28], we observe a d -like band with a binding energy of about 1.7 eV at X , shown in Figs. 2(a) and (b). In all previous work [9–14, 28], this deep state has been interpreted as the bulk band that hybridizes with the f -orbital multiplet to open the bulk gap at low temperature.

While our data are compatible with the existence of such a three-dimensional band, we find clear evidence that the prominent parabolic dispersion observed here and previously [9–14, 28] is a surface state: Photon energy dependent measurements unequivocally show the existence of a two-dimensional state at binding energies well beyond that of the shallowest f -orbital multiplet (${}^6H_{5/2}$). The photoemission intensity on both the $\Gamma-X-M$ and the $X-M-R$ planes is shown in Figs. 2(c) and (d-e) respectively. While traces of the three-dimensional d -band around X can be observed—most prominently in Fig. 2(d)—the vertical features in all three panels provide clear evidence of a state that does not display a dependence with the electron wave vector perpendicular to the surface k_{\perp} .

Denlinger et al. have also attempted to determine the dimensionality of the electronic structure beyond the f -orbital multiplet using photon energy dependent ARPES measurements [14]. In contrast to our findings, they do not find

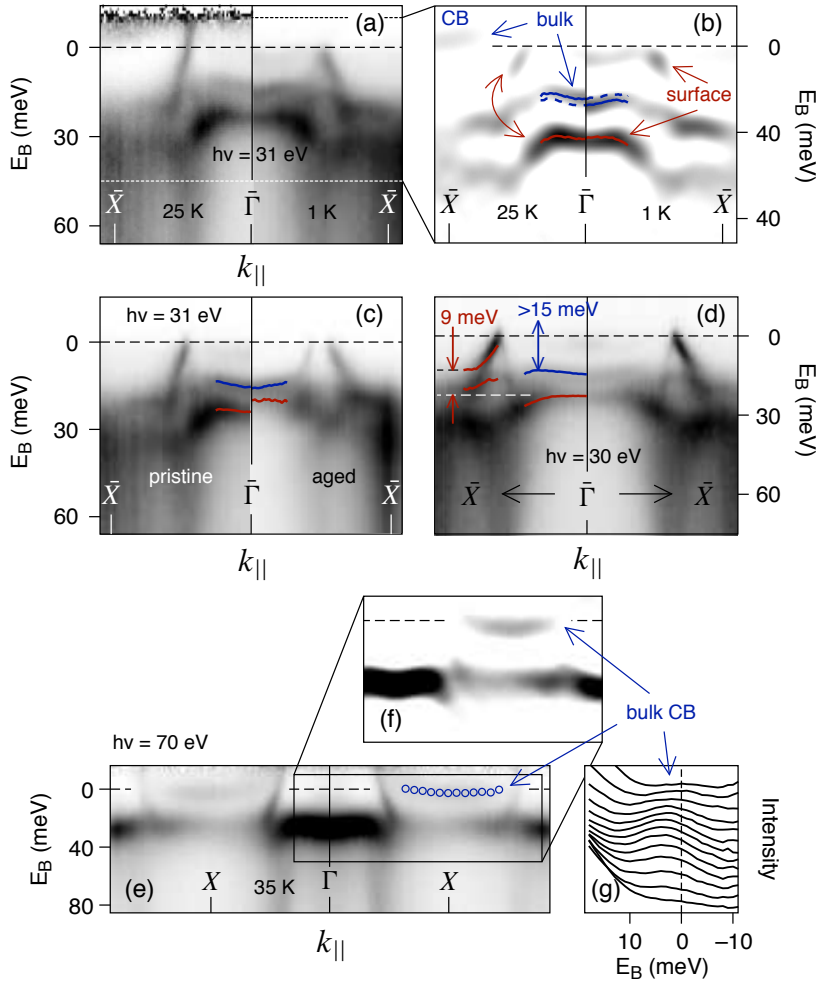


Figure 3. Bulk and surface d - f hybridization. (a–c) Evolution of bulk and surface features as a function of temperature and sample ageing. (b) Second derivative (d^2I/dE^2) of the indicated energy range of (a). (e–g) Dispersion of the bulk conduction band (CB) near X . (f) Second derivative (d^2I/dE^2) of the indicated area. (g) Conduction band as spectra. Photoemission intensity in the left half of (a) and in (e–g) is divided by the Fermi-Dirac distribution at the corresponding temperature. Solid lines in (b–d) and markers in (e) indicate maxima of energy distribution curve fits. Dashed lines in (b) indicate the positions of maxima in the other half of the graph. Intensity in left and right halves of (d) and (e) mirrored about $k_{||} = 0$. All measurements with p -polarized light.

evidence of the two-dimensional state below the f -orbital multiplet. We attribute this discrepancy to their choice of binding energy that is relatively close to the hybridization region. We observe features not dispersing with k_{\perp} at all binding energies sufficiently far away from the multiplets, where the signal is not dominated by the f intensity. We further note that the photoemission intensity from the surface state varies strongly with light polarization and is suppressed with s -polarization in the given geometry.

The existence of this deep, massive surface state invalidates the premise of earlier studies that the elliptical Fermi surface contour around \bar{X} can be attributed to an independent in-gap state. In fact, due to its group velocity, the massive band at \bar{X} will inevitably persist above the ${}^6H_{5/2}$ f -orbital multiplet. This provides an alternative, trivial explanation for the elliptical Fermi surface contour around \bar{X} reported in all ARPES experiments. In the following we will detail how this metallic feature springs from the deep surface state at \bar{X} .

In accordance with the results of Min et al. [13] and Denlinger et al. [14], we observe how the bulk conduction band appears to move above the Fermi level upon cooling below a temperature of about 30 K. This is illustrated in Fig. 3(a) and (b). Simultaneously with the disappearance of the bulk conduction band at \bar{X} we find that the upper maximum of the f multiplet at $E_B \sim 15$ meV around $\bar{\Gamma}$, shifts downwards when the temperature is lowered from 25 to 1 K. The latter band can thus be identified as the bulk valence band that is pushed to higher binding energy as the size of the hybridization gap increases. We tentatively assign the f -level with nearly identical dispersion below it to the

surface counterpart of this band, because it does not show this temperature effect. This assignment is corroborated by studying the effect of sample ageing on the surface electronic structure, detailed in Fig. 3(c). Exposure of a freshly cleaved surface to the ultrahigh vacuum residual gas for 24 hours apparently gives rise to p -doping of the surface region: The binding energy of all surface related features is reduced by 5 – 10 meV. We can thus more confidently assign the f level with the larger binding energy to the surface and conclude that the $4f$ level in the pristine sample displays a surface core level shift of about 10 meV. With this assignment we can disentangle the contributions from bulk and surface to the photoemission spectra and arrive at an estimate for the hybridization strength in both cases. The binding energy of the bulk f -level around $\bar{\Gamma}$ provides a lower limit for the indirect bulk hybridization gap of about 15 meV. Near \bar{X} we observe that the metallic surface state hybridizes with an f -level at about 13 meV. Interpreting this state as the surface analogue of the bulk conduction band, we conclude that the surface hybridization gap amounts to ~ 9 meV, see Fig. 3(d).

This observation completes our picture of the surface electronic structure of SmB_6 . We find that hybridization is not only weaker at the surface, the gap is also shifted away from the Fermi level due to a surface core level shift of the $4f$ level. Consequently, the surface remains metallic at the lowest temperature. Similarly, Frantzeskakis et al. suggested that the chemical potential does not lie in the hybridization gap and that therefore the metallic state at \bar{X} is not an in-gap topological surface state but the continuation of the bulk d -band [28]. We can agree with the spirit of their conclusion, but note that it only applies to the surface region and not to the bulk.

Regarding the tiny size of the $4f$ surface core level shift, we note that for the B-terminated surface the chemical environment of the surface Sm atoms is nominally identical to the bulk. As a consequence, the $4f$ surface shift is naturally much smaller than that of rare earth metals where the coordination of surface atoms is strongly reduced compared to their bulk counterparts. In those cases, the shift amounts to several 100 meV. We observe a shift of that order of magnitude for the Sm atoms in the outermost layer of Sm-terminated surfaces (Fig. 1(j)). In this context we also note that the surface ${}^6H_{5/2}$ multiplet directly confirms the presence of Sm^{2+} ions at the surface. This result clearly conflicts with the assertion by Phelan et al., based on X-ray absorption spectroscopy, that the surface consists of Sm^{3+} exclusively [36].

Finally, we mention that a change of the d - f hybridization strength at the surface is not unusual and has been observed with ARPES for other heavy fermion systems [37]. As a possible cause for weaker surface hybridization in the present system, we point out that the application of pressure is known to suppress the bulk gap of SmB_6 [38]. Experimental determinations of the surface structure are lacking so far but calculations indicate an appreciable reduction of the separation between the outermost layers [39].

DISCUSSION

In summary, we find evidence that strongly supports the existence of two trivial metallic states that can account for the observed surface conductivity of SmB_6 . In Fig. 4, we graphically contrast the theoretically predicted scenario (a) with the interpretation based on our experimental results (b). Instead of topological surface states giving rise to Dirac cones at $\bar{\Gamma}$ and \bar{X} , we find a massive free electron-like state at $\bar{\Gamma}$, and the occupied conduction band of the surface d - f hybrid at \bar{X} .

While our data are compatible with all previous experimental reports, there are two rather strong observations apparently supporting the topological prediction that we will try to counter in the following. Firstly, Xu et al. have found the helical spin texture expected for a topological surface state with spin-resolved ARPES [12]. However, we point out that the possibility of a spin-polarized Rashba-split state of considerable extent in k -space, such as we observe at $\bar{\Gamma}$, has not been considered in the interpretation of their results. We further note that the energy resolution of state-of-the-art spin-resolved ARPES is insufficient to distinguish between the surface state and the f -orbital multiplet. This issue is exacerbated by the study's heavy reliance on circularly polarized light, which is known to give rise to strongly spin-polarized emission from the f -orbital multiplet [40]. Moreover, it is not clear why spin-resolved measurements on YbB_6 by the same group yield a topological spin texture for the surface state at \bar{X} [41], while a strong case can be made that the dispersion is that of a trivial state [42]. The second, although somewhat indirect, experimental result in support of topological surface states in SmB_6 is provided by impurity doping experiments. Kim et al. find that the residual low temperature conductivity disappears upon doping with magnetic Gd impurities but not with non-magnetic Y [27], compatible with the expectation that a gap should open at the Dirac point of a topological surface state upon breaking time reversal symmetry. However, we point out that such disordered magnetic moments do not open a gap at the Dirac point of the established topological insulator Bi_2Se_3 as has been shown for Fe and Gd [43]. We therefore conclude that these arguments in favor of the topological insulator phase in SmB_6 are insufficiently strong to challenge our trivial interpretation.

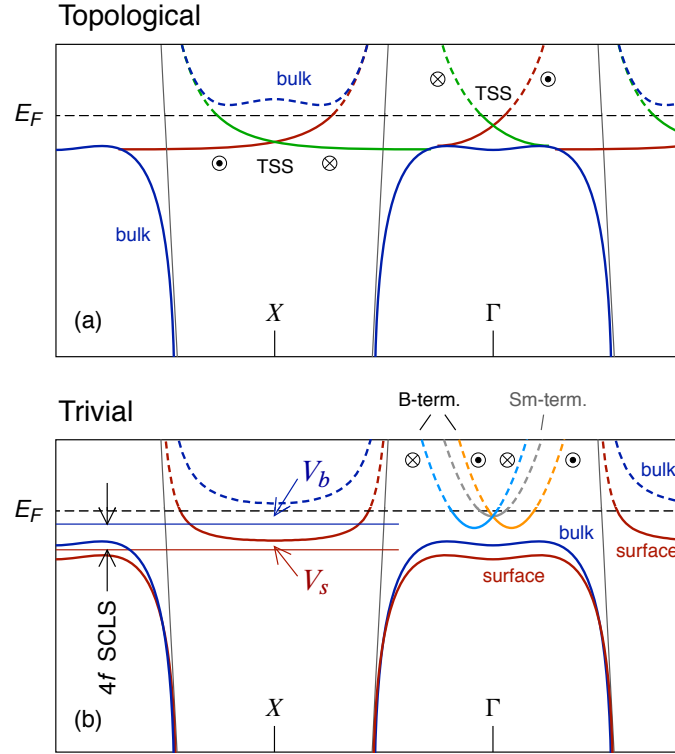


Figure 4. (a) Sketch of the situation predicted by theory, and (b) scenario based on the present experiment. Instead of the predicted topological surface states (TSS), we observe a massive surface state with a spin degeneracy that can be lifted by the Rashba effect at $\bar{\Gamma}$. Figure (b) further illustrates how the prominent Fermi surface feature at \bar{X} arises due to a surface core level shift (SCLS) of the $4f$ level and a difference in hybridization strength V between bulk and surface. Unhybridized bands are indicated by thin solid lines.

What could explain the chasm between our interpretation and the theoretical prediction? We iterate that the topological classification of SmB_6 hinges on a band inversion at the X -point. Regardless of the applied method, the calculated conduction band is found to have a W -shaped dispersion at X indicative of the inversion [5–7, 39]. Within the limits of the k_{\perp} resolution achievable in ARPES, we observe a simple U -shape instead, as shown in Fig. 3(e–g).

We note with respect to the Rashba splitting of the $\bar{\Gamma}$ state that, in spite of the small Rashba parameter α_R , the observed splitting in momentum space ($\Delta k_{\parallel} = 0.08 \text{ \AA}^{-1}$) easily exceeds that of the largest known semiconductor Rashba systems [44]. Heavy-fermion systems could thus be a fruitful source of materials with very large Rashba splitting. Relying on the effective mass instead of the Rashba parameter to achieve the splitting facilitates control over the splitting by means of relatively small changes to the surface potential.

With regard to the surface termination, we note that we observe apparently pure B and Sm terminations which is surprising since this would lead to divergence of the electrostatic surface energy for bulk truncated structures. We cannot provide a comprehensive picture of the different terminations on the basis of our results and the current literature. The umklapp features we observe for either termination are compatible with the finding by Rößler et al. that most of the surface area exhibits a (2×1) reconstruction [45]. However, an interpretation [45] in terms of missing Sm rows is clearly incompatible with the spectra in Fig. 1(i–l). We note, though, that both the metallic surface states at $\bar{\Gamma}$ and \bar{X} are present regardless of the termination. This clearly indicates that they are not confined to the outermost surface layer, but enjoy the chemical protection by at least one B layer. We suggest that this isolation from the environment can account for the observed robustness [25] of the surface conductivity.

We thank Prof. B. Lake for continuous support of the present activity. The authors acknowledge financial support by Deutsche Forschungsgemeinschaft through SPP 1666, by "Impuls- und Vernetzungsfonds der Helmholtz-Gemeinschaft" through Helmholtz-Russia Joint Research Group no. 408 and Helmholtz Virtual Institute "New states of matter and their excitations". The authors also acknowledge the support of Slovak grant agency projects VEGA 2/0106/13, APVV 0132-11, and CFNT MVEP of the Slovak Academy of Sciences.

-
- [1] M. Z. Hasan and C. L. Kane, Rev. Mod. Phys. **82**, 3045 (2010); B. A. Bernevig and T. L. Hughes, *Topological Insulators and Topological Superconductors* (Princeton University Press, 2013).
- [2] Y. Ando, J. Phys. Soc. Jpn. **82**, 102001 (2013).
- [3] A. Shitade, H. Katsura, J. Kuneš, X.-L. Qi, S.-C. Zhang, and N. Nagaosa, Phys. Rev. Lett. **102**, 256403 (2009); H.-M. Guo and M. Franz, *ibid.* **103**, 206805 (2009).
- [4] M. Dzero, K. Sun, V. Galitski, and P. Coleman, Phys. Rev. Lett. **104**, 106408 (2010).
- [5] T. Takimoto, J. Phys. Soc. Jpn. **80**, 123710 (2011).
- [6] F. Lu, J. Zhao, H. Weng, Z. Fang, and X. Dai, Phys. Rev. Lett. **110**, 096401 (2013).
- [7] V. Alexandrov, M. Dzero, and P. Coleman, Phys. Rev. Lett. **111**, 226403 (2013).
- [8] B. Roy, J. D. Sau, M. Dzero, and V. Galitski, Phys. Rev. B **90**, 155314 (2014).
- [9] M. Neupane, N. Alidoust, S.-Y. Xu, T. Kondo, Y. Ishida, D. J. Kim, C. Liu, I. Belopolski, Y. J. Jo, T.-R. Chang, H.-T. Jeng, T. Durakiewicz, L. Balicas, H. Lin, A. Bansil, S. Shin, Z. Fisk, and M. Z. Hasan, Nat. Comm. **4**, 2991 (2013).
- [10] J. Jiang, S. Li, T. Zhang, Z. Sun, F. Chen, Z. R. Ye, M. Xu, Q. Q. Ge, S. Y. Tan, X. H. Niu, M. Xia, B. P. Xie, Y. F. Li, X. H. Chen, H. H. Wen, and D. L. Feng, Nat. Comm. **4**, 3010 (2013).
- [11] N. Xu, X. Shi, P. K. Biswas, C. E. Matt, R. S. Dhaka, Y. Huang, N. C. Plumb, M. Radović, J. H. Dil, E. Pomjakushina, K. Conder, A. Amato, Z. Salman, D. M. Paul, J. Mesot, H. Ding, and M. Shi, Phys. Rev. B **88**, 121102 (2013).
- [12] N. Xu, P. K. Biswas, J. H. Dil, R. S. Dhaka, G. Landolt, S. Muff, C. E. Matt, X. Shi, N. C. Plumb, M. Radović, E. Pomjakushina, K. Conder, A. Amato, S. V. Borisenko, R. Yu, H. Weng, Z. Fang, X. Dai, J. Mesot, H. Ding, and M. Shi, Nat. Comm. **5**, 4566 (2014).
- [13] C.-H. Min, P. Lutz, S. Fiedler, B. Y. Kang, B. K. Cho, H. D. Kim, H. Bentmann, and F. Reinert, Phys. Rev. Lett. **112**, 226402 (2014).
- [14] J. D. Denlinger, J. W. Allen, J.-S. Kang, K. Sun, J. W. Kim, J. H. Shim, B. I. Min, D.-J. Kim, and Z. Fisk, arXiv (2013), 1312.6637v1.
- [15] G. Li, Z. Xiang, F. Yu, T. Asaba, B. Lawson, P. Cai, C. Tinsman, A. Berkley, S. Wolgast, Y. S. Eo, D.-J. Kim, C. Kurdak, J. W. Allen, K. Sun, X. H. Chen, Y. Y. Wang, Z. Fisk, and L. Li, Science **346**, 1208 (2014).
- [16] J. C. Cooley, M. C. Aronson, Z. Fisk, and P. C. Canfield, Phys. Rev. Lett. **74**, 1629 (1995).
- [17] K. A. Kikoin and A. S. Mischenko, J Phys-Condens Mat **7**, 307 (1995).
- [18] T. Kasuya, J. Phys. Soc. Jpn. **65**, 2548 (1996).
- [19] P. S. Riseborough, Adv Phys **49**, 257 (2000).
- [20] N. E. Sluchanko, V. V. Glushkov, B. P. Gorshunov, S. V. Demishev, M. V. Kondrin, A. A. Pronin, A. A. Volkov, A. K. Savchenko, G. Grüner, Y. Bruynseraede, V. V. Moshchalkov, and S. Kunii, Phys. Rev. B **61**, 9906 (2000).
- [21] E. E. Vainshtein, S. M. Blokhin, and Y. B. Paderno, Sov. Phys. Solid State **6**, 2318 (1965).
- [22] A. Menth, E. Buehler, and T. H. Geballe, Phys. Rev. Lett. **22**, 295 (1969).
- [23] J. C. Nickerson, R. M. White, K. N. Lee, R. Bachmann, T. H. Geballe, and G. W. Hull, Jr, Phys. Rev. B **3**, 2030 (1971).
- [24] J. W. Allen, B. Batlogg, and P. Wachter, Phys. Rev. B **20**, 4807 (1979).
- [25] S. Wolgast, Ç. Kurdak, K. Sun, J. W. Allen, D.-J. Kim, and Z. Fisk, Phys. Rev. B **88**, 180405 (2013).
- [26] X. Zhang, N. P. Butch, P. Syers, S. Ziemak, R. L. Greene, and J. Paglione, Phys. Rev. X **3**, 011011 (2013).
- [27] D. J. Kim, J. Xia, and Z. Fisk, Nat. Mater. **13**, 466 (2014).
- [28] E. Frantzeskakis, N. de Jong, B. Zwartsenberg, Y. K. Huang, Y. Pan, X. Zhang, J. X. Zhang, F. X. Zhang, L. H. Bao, O. Tegus, A. Varykhalov, A. de Visser, and M. S. Golden, Phys. Rev. X **3**, 041024 (2013).
- [29] We find that samples cleave with two distinct terminations as is further described in the Methods section.
- [30] F. Gerken, J. Phys. F **13**, 703 (1983).
- [31] See e.g., New J. Phys., Focus on the Rashba Effect.
- [32] Y. L. Chen, J. G. Analytis, J. H. Chu, Z. K Liu, S. K. Mo, X. L. Qi, H. J. Zhang, D. H. Lu, X. Dai, Z. Fang, S. C. Zhang, I. R. Fisher, Z. Hussain, and Z.-X. Shen, Science **325**, 178 (2009).
- [33] G. Nicolay, F. Reinert, S. Hüfner, and P. Blaha, Phys. Rev. B **65**, 033407 (2001).
- [34] G. Bihlmayer, Y. M. Koroteev, P. M. Echenique, E. V. Chulkov, and S. Blügel, Surface Science **600**, 3888 (2006).
- [35] A. Varykhalov, D. Marchenko, M. R. Scholz, E. D. L. Rienks, T. K. Kim, G. Bihlmayer, J. Sánchez-Barriga, and O. Rader, Phys. Rev. Lett. **108**, 066804 (2012).
- [36] W. A. Phelan, S. M. Koohpayeh, P. Cottingham, J. W. Freeland, J. C. Leiner, C. L. Broholm, and T. M. McQueen, Phys. Rev. X **4**, 031012 (2014).
- [37] D. V. Vyalikh, S. Danzenbächer, Y. Kucherenko, C. Krellner, C. Geibel, C. Laubschat, M. Shi, L. Patthey, R. Follath, and S. Molodtsov, Phys. Rev. Lett. **103**, 137601 (2009).
- [38] S. Gabáni, E. Bauer, S. Berger, K. Flachbart, Y. Paderno, C. Paul, V. Pavlík, and N. Shitsevalova, Phys. Rev. B **67**, 172406 (2003).
- [39] J. Kim, K. Kim, C.-J. Kang, S. Kim, H. C. Choi, J.-S. Kang, J. D. Denlinger, and B. I. Min, Phys. Rev. B **90**, 075131 (2014).
- [40] S. Suga, K. Sakamoto, T. Okuda, K. Miyamoto, K. Kuroda, A. Sekiyama, J. Yamaguchi, H. Fujiwara, A. Irizawa, and T. Ito, J. Phys. Soc. Jpn. **83** (2013).
- [41] N. Xu, C. E. Matt, E. Pomjakushina, J. H. Dil, G. Landolt, J. Z. Ma, X. Shi, R. S. Dhaka, N. C. Plumb, M. Radović, V. N. Strocov, T. K. Kim, M. Hoesch, K. Conder, J. Mesot, H. Ding, and M. Shi, arXiv (2014), 1405.0165v1.

- [42] E. Frantzeskakis, N. de Jong, J. X. Zhang, X. Zhang, Z. Li, C. L. Liang, Y. Wang, A. Varykhalov, Y. K. Huang, and M. S. Golden, *Phys. Rev. B* **90**, 235116 (2014).
- [43] T. Valla, Z. H. Pan, D. Gardner, Y. S. Lee, and S. Chu, *Phys. Rev. Lett.* **108**, 117601 (2012); M. R. Scholz, J. Sánchez-Barriga, D. Marchenko, A. Varykhalov, A. Volykhov, L. V. Yashina, and O. Rader, *ibid.* **108**, 256810 (2012).
- [44] K. Ishizaka, M. S. Bahramy, H. Murakawa, M. Sakano, T. Shimojima, T. Sonobe, K. Koizumi, S. Shin, H. Miyahara, and A. Kimura, *Nat. Mater.* **10**, 521 (2011); P. D. C. King, R. C. Hatch, M. Bianchi, R. Ovsyannikov, C. Lupulescu, G. Landolt, B. Slomski, J. H. Dil, D. Guan, J. Mi, E. D. L. Rienks, J. Fink, A. Lindblad, S. Svensson, S. Bao, G. Balakrishnan, B. B. Iversen, J. Osterwalder, W. Eberhardt, F. Baumberger, and P. Hofmann, *Phys. Rev. Lett.* **107** (2011).
- [45] S. Rößler, T. H. Jang, D. J. Kim, L. H. Tjeng, Z. Fisk, F. Steglich, and S. Wirth, *Proc. Natl. Acad. Sci.* **111**, 4798 (2014).
- [46] J. D. Denlinger, J. W. Allen, J.-S. Kang, K. Sun, B.-I. Min, D.-J. Kim, and Z. Fisk, *arXiv* (2013), 1312.6636v2.

Materials and Methods

SmB₆ powder has been synthesized by borothermal reduction of Sm₂O₃ with metallic B powder under vacuum at 1900 K. The powder was pressed to rods that were sintered under vacuum at 2000 K. The sintered rods of ~ 8 mm diameter and 60 mm length then have been used for single crystal growth with an inductive, crucible free floating zone technique under 0.4 MPa Ar pressure. The starting components were amorphous natural B and Sm₂O₃. The purity was 99.9% and 99.996% in the case of B and Sm₂O₃, respectively. Single crystals with a diameter of typically 6 mm and a length of up to 40 mm were grown using [100] oriented seeds. The growth procedure was repeated twice to remove any porosity from the starting feed rods. During the first passage the crystallization rate was 1 mm/min which gave the primary crystal without pores. At the end of the first passage the melting zone was frozen and the crystal was zone-melted again to the opposite side with a crystallization rate of 0.4 mm/min while rotating the crystal with 5 rpm. Powder X-ray diffraction patterns of the crushed SmB₆ crystal revealed the presence of the SmB₆ only. Moreover, Laue back scattering patterns from both ends of the crystal shows a single crystal with [100] orientation. The crystal employed for the present ARPES experiments showed a residual resistance of $R(1\text{K})/R(300\text{K}) = 5.3 \times 10^4$. Oriented slabs with length up to 5 mm and typical cross section of $1 \times 1 \text{ mm}^2$ have been cut for the ARPES experiments. The orientation was again verified using X-ray Laue diffraction which gave sharp reflections and did not show any twinning.

Samples were cleaved in ultrahigh vacuum ($< 10^{-10}$ mbar) at temperatures below 40 K. The crystal is found to cleave with two distinct terminations: An apparently purely B terminated surface which is characterized by a complex B 1s spectrum, shown in Fig. 1(i), and a relatively simple valence band spectrum which contains the Sm²⁺ f -orbital multiplet ($4f^6 \rightarrow 4f^5$ photoemission transition) [Fig. 1(j)]. The other termination apparently exposes Sm atoms exclusively, evidenced by the simple B 1s spectrum and the additional surface components in the valence band. Similar variations of the valence band spectrum have recently been observed [46]. All results presented in this work were obtained with surfaces of which the size of regions with a single termination exceeds the size of the synchrotron beam profile. Regardless of the termination, we observe the effect of a potential with twice the lattice constant, presumably due to several domains of a (2×1) surface reconstruction reported in scanning tunneling microscopy [45].

Photoemission experiments were performed with the 1³ ARPES end-station at the UE112-PGM2b beamline of BESSY II. Data at $h\nu = 31$ eV were obtained with an energy resolution of 3 meV. A sample temperature of 1 K is used unless indicated otherwise. k_{\perp} values are calculated assuming a free electron final state using an inner potential of 14 eV.